Global Scientific and Academic Research Journal of Multidisciplinary Studies
ISSN: 2583-4088 (Online)
Frequency: Monthly
Published By GSAR Publishers
Journal Homepage Link- https://gsarpublishers.com/journals-gsarjms-home/

Synthesis and Characterization of La-Doped BNBT Lead-Free Ceramics with Enhanced Piezoelectric and Dielectric Properties

By

Asfand Yar Shafique[1*], Mehwish Nazar[2], Maryam Liaqat[3], Fawad Ahmad Khan[4], Saeed Ahmad[5] Waheed Zaman khan[6]

[1]Department of Physics, Qurtuba University of Science and IT, Peshawar 25000, Pakistan.
[2]School of Science, Department of Chemistry University of Management and Technology, Lahore, Pakistan
[3]College of Electronics and Information Engineering, Shenzhen University, Shenzhen 518060, China
[4]Department of Physics, Abdul Wali Khan University, Mardan, 23200 Khyber Pakhtunkhwa, Pakistan
[5]Department of Physics, Abdul Wali Khan University, Mardan, 23200 Khyber Pakhtunkhwa, Pakistan
[6]Department of Physics, Division of Science and Technology, University of Education, Lahore, Punjab 54770, Pakistan.

Article History

Received: 15/02/2025
Accepted: 21/02/2025
Published: 24/02/2025

Vol – 4 Issue –2

PP: - 56-67

DOI:10.5281/zenodo.15046638

Abstract

The present work deals with the synthesis of $[(Na_{0.5}Bi_{0.5})_{0.94}Ba_{0.06}]_{1-x}La_xTiO_3$ with the method of conventional solid-state reaction with the composition of BNLBT in which the "x" has value 0.02. These ceramics show large piezoelectric and dielectric properties with the addition of La into BNT-BT. X-ray diffraction analysis for 0.02mol% shows a single perovskite rhombohedral structure without other phases. The surface morphology is examined by FE-SEM, where the average grain size is calculated at 1.08 to 2.02 µm. The maximum dielectric constant observed at a frequency of 1MHz was 3980 for a ratio of 0.02 mol%, while T_d shifted to almost room temperature. A low loss factor (tanδ) of less than 10% was observed for 0.02mol% under 1 kHz, 10 kHz, and 100 kHz. For BNBT-3La, the huge maximum strain S_{max} is 0.27% with a high normalized strain d^*_{33}= 387 pm/V under 70 kV/cm at room temperature. A thin P-E loop was obtained for BNBT-La 0.02mol%, from the P-E loop, huge remnant polarization P_r= 20.91 µC/cm^2, P_{max}= 42.58 µC/cm^2, and E_c= 16 kV/cm was observed.

Keywords: *Lanthanum-Doped BNBT Ceramics, Lead-Free Piezoelectric Materials, Dielectric and Ferroelectric Properties, Perovskite Structure Optimization, Electromechanical Coupling Efficiency*

1. Introduction

In this chapter, we have a general discussion about lead-free ceramics and the historical background of the first piezoelectric material, BT, along with structure analysis. In the present chapter, it is explained how the scientists were thinking about the BNT system and its derivatives discussed briefly.

1.1 Barium Titanate

The electromechanical industry is facing some basic challenges to the development of advancement of technologies because of the limited resources of core materials. Applications due to a huge range of consumer areas require future equipment with reduced size and, low power consumption, high levels of functionality. We need to develop new materials with better qualities like high dielectric constant, for piezoelectric sensors and actuators, high piezoelectric response with a low temperature is necessary.

In 1940's the several materials were studied for their ferroelectric properties or vignette-electric, three groups of these substances are Rochelle salt, potassium dihydrogen phosphate, and barium titanate. All these three substances were similar at necessarily high temperatures, but the dielectric constant was very large. They showed pure substance in these groups, where only barium titanate with lead or strontium titanate showed similar properties [1].

Ferroelectricity was discovered in barium titanate in the early 1940s, and researchers are still studying that material. The Ti^{4+} ion in $BaTiO_3$ is slightly displaced from the middle of the cube, which leads to an electric dipole due to the separation between the mid of the -ve and +ve charges in the unit cell. The structure of ABO_3 barium titanate ($BaTiO_3$) is shown in

*Corresponding Author: **Asfand Yar Shafique**

Figure 1.1. Ideally, the entire unit cell should have a polarization in the same direction as the ceramics. The same polarization is located in the small regions; these small regions are called domains. The Curie temperature (T_c) for the $BaTiO_3$ (~120°C), each domain contains a different direction of polarization because of the random orientation of every domain. By applying an external electric field, the domain tends to be oriented in the direction of the external field. The general formula of perovskite structure is ABO_3, where barium (Ba^{+2}) and titanium (Ti^{+4}) are cations and oxygen (O^{-2}) is an anion. The Titanium cations are located in the octahedral vacuum created by the oxygen (O^{-2}) anions in the adjacent layers. Because this makes a cubic structure within the layers, BT has three-phase transmission, if the temperature falls, it changes from cubic phase to tetragonal (Te), Orthorhombic (Or), Rhombohedral (Rh) phase [2-3].

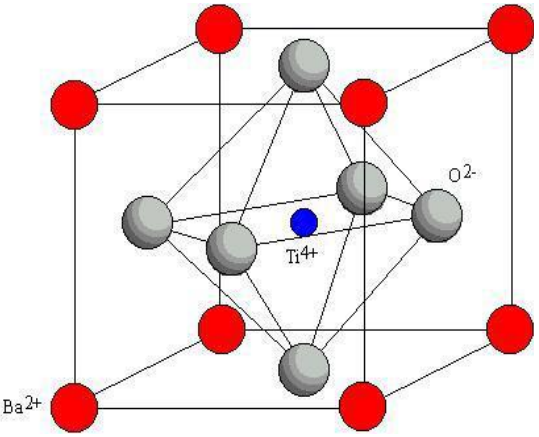

Figure 1.1: The crystal structure of barium titanate ($BaTiO_3$).

1.2 Sodium Bismuth Titanate (BNT)

Several researchers around the world are keenly busy in ferroelectric research to make idealized alternatives to lead-based ceramics. $Bi_{0.5}Na_{0.5}TiO_3$ (BNT) is considered to be a brilliant applicant for lead-free ferroelectric material. BNT was discovered for the first time by *Smolenskii et al*. in 1960 . In BNT, the "Bi" and "Na" cations are placed on the edge of the unit cell. The "O" cation stays at the face centers to form an octahedral, and the "Ti" cation is in the middle of the "O" octahedra. The structure of a crystal of BNT and phase transition at different temperatures was studied by *Jones et al.* in 2002 [4]. It is obtained that BNT ceramics show a large dielectric loss and weak piezoelectric properties due to a high coercive field (Ec = 73 kV/cm) because BNT is difficult to polarize. After this polling problem and to enhance the piezoelectric properties of BNT, the researcher has to think about various BNT-based solid solutions with rhombohedral (Rh) to tetragonal (Te) in MPB [5]. To enhance the piezoelectric properties within MPB, the different tetragonal compounds doped into BNT, such as $SrTiO_3$, $BiFeO_3$, $PbTiO_3$, and $NaNbO_3$. *Li et al.* have stated the dielectric property and piezoelectric response of BNT- $NaNbO_3$ ceramics. The samples in the composition range of 0.01 to 0.02 were found to show d_{33} = 80 – 88pC/N [6]. BNT-KBT relaxor showed as the cation discord due to Na^{+1}, K^{+1}, and Bi^{3+} at A-site. In the tetragonal system, the ceramics show antiferroelectric because of loosely packed A-site cations [7]. *Yoshii et al.* successfully prepared the lead-free ceramics La-doped BNT-BKT solid solution with less decrease in depolarization temperature T_d= 219°C and d_{33}= 153pC/N and preferred this solution for the application of actuators [8] in KN doped BNT-BT ceramics system prepared by sol-gel technique and hydrothermal technique. XRD investigated that BNTBT-KN has a perovskite phase, but with the increasing of KN doping, the rhombohedral phase reduced and at room temperature shows a large dielectric constant [9]. A BT-BMT new lead-free ceramic system to enhance the Curie temperature of BT introduced by *Wada et al.*, the dielectric property of BT-BMT system shows relaxor behavior for $_{0.5}$BT-$_{0.5}$BMT Dielectric maximum temperature as high T_c=360°C and piezoelectric constant for 0.4BT-0.6BMT as 60pC/N [10]. *Takenaka et al.* obtained The BNT- 6% BT composition for d_{33}~125pC/N, k_{33}= 55% and tangent loss factor 1.3%, *T*c and FE to AFE transition temperature reduced at MPB [11]. *Ranjan et al.* studied the dielectric properties of (1-x)NBT- xBT with ($0 \leq x \leq 0.10$) and observed the structure of BNT-BT Rhombohedral at x=0.05 and where above this forms cubic [12]. Co-doped La^{+3} and Ta^{+5} in BNT-0.06BT show no change in the lattice of the crystal, and a solution exists in the MPB region, the depolarization temperature observed decreases [13]. Ta^{+5} doped BNT-BT were successfully prepared and investigated by XRD that Ta^{+5} doped BNT-BT composition is in MBP region or near to it, where lattice parameter slightly changed with Ta^{+5} doped, observed the grain size of the decreases from 1.82µm to 1.62µm and Dielectric constant increases with an increase in dopant [14]. Sm^{3+} doped in BNT-BT prepared by the solid-state conventional route. For $0.94(Na_{0.5}Bi_{0.5})$, TiO_3-$0.06BaTiO_3$-$x Sm^{3+}$ sample of x=0.003 shows good d_{33}= 202pC/N, which refers to the doping of Sm^{3+} in small amounts enhanced piezoelectric property. The ceramics show great absorption at 407nm, which is similar to emission wavelength LED chips near ultraviolet and preferred BNT-BT doped Sm^{3+} ceramics for the White light emitting diode [15]. To improve the sintering performance and piezoelectric property in BNT-BT, Lithium (Li) was added in BNT-BT observed the piezoelectric constant d_{33}= 210pC/N, which shows great improvement in doped and undoped, as well as loss tangent factor = 4.2% [16].

The structure and phase transition behavior of La-doped BNT ceramics were studied by Lee *et al.* The lanthanum combination creates A-site as well as B-site vacancies. In A-site situations, the phase transition close to 200 °C becomes noticeable and contributes to the insufficient antiferroelectric phase, but La-doped B-site situations do not contribute to the insufficient phase [17]. La was added into the BNT system, with the increasing dopant, the dielectric constant peak extended, and the A-sites position disturbed. Comparison between doped and undoped BNT system, P_r and E_c reduced with La^{+3} x= 0.07. But La^{+3} added BNT ceramics that make it easy to control the polarity with a small electric field [18]. *Mercadelli et al*. Ba^{2+} doped BNT lead-free systems were prepared by sol-gel technique in 2008 [19]. *Qu et al.* prepared

*Corresponding Author: **Asfand Yar Shafique**

a Ba^{2+} doped BNT solid solution and positively experimentally explained that ions in the A-site exchanged by Ba^{2+} and structure slightly changed, which is a great improvement in BNT solutions for enhancement in dielectric properties [20]. *Rao et al.* Ba^{2+} added in the BNT system and observed theoretical value shows a high density of BNBT with a low disturbance in a lattice structure. With increasing the dopant Ba^{2+} in BNT, the rate of T_m and T_d is decreased, where the loss factor (tanδ) of Ba^{2+} doped BNT ceramics is observed to be very low, which represents little loss material [21]. *Chen et al.* observed that BNBT relaxor behavior shows at high temperatures with increasing the value of dopant [22].

Fu et al. added $BiAlO_3$ (BA) in BNBT and observed pure perovskite structure, where x=0.005 shows MPB. Electrical properties upgraded in BNBT with increasing BA. At room temperature, the composition of (1-x)BNBT6–xBA at x=0.0225 the piezoelectric constant d_{33}=204pC/N and dielectric property ε_r=1687 obtained [23]. *Zhao et al.* introduce a new dopant $(Al_{0.5}Nb_{0.5})^{4+}$ in BNBT for enhanced energy storage applications. Within the MBP, a single perovskite phase was observed, with increasing dopant T_m peaks larger. $(Al_{0.5}Nb_{0.5})^{4+}$ at x= 0.04 P_r and E_c drops, where P-E loos becomes thin [24]. $(Fe_{0.5}Nb_{0.5})^{4+}$ added in the BNBT for increasing the piezoelectric constant and observed unipolar stain d^*_{33}=600pm/V *Cheng et al.* [25]. $(Pr_{0.5}Nb_{0.5})^{4+}$ add in BNBT by Wang et al. observed comparatively pure BNT and BNBT-PN with no improvement observer in P_r but d_{33} enhanced from 121pC/N to 221pC/N dopant x=0.005 [26]. *Hao et al.* doped $(Fe_{0.5}Ta_{0.5})$ in the BNBT system, obtained d^*_{33}=500pm/V at x=0.06 [27]. *Li et al.* (Fe, Sb) added in the BNBT ceramics system, BNBT-FS at x=0.015, the disturbance located into the FE long-range order and observed d^*_{33}=454pm/V [28]. *Zheng et al.* modified BNT with La^{3+} and Ba^{2+} and observed that T_d falls with increasing the concentration of dopant x= 0-0.04 with piezoelectric constant d_{33}= 196pC/N. The concentration of x > 0.06 shows a fall in the piezoelectricity of BNBT and weak dielectric properties [29].

2. Experimental Techniques

This section presents the basic principles, techniques, and synthesis routes employed for the fabrication of materials in this research. It also discusses the characterization methods used to analyze the materials, including X-ray Diffraction (XRD), dielectric measurements, Scanning Electron Microscopy (SEM), and piezoelectric response evaluations.

2.1 Synthesis Routes

Ceramics are the most important part of industries, like the electrical industry, etc. the methodology for preparing ceramics has an important role in the enhancement of properties [30-31]. New technique shows awesome results as well as making products in the affordable range. The synthesis technique is directly related to the properties of the material or ceramics [32]. The logic behind the different techniques is to explain the properties and examine the effect on the materials in various parameters. There are two forms of ferroelectric material, monocrystalline and polycrystalline, but it is very hard to prepare monocrystalline. Relatively, the polycrystalline form is more stable than the monocrystalline form and is easy to synthesize [33].

2.1.1 Types of Techniques

From long ago, ceramics were prepared by simply heating, but nowadays, the ceramics property has changed, and a large improvement has been seen just because of the processing techniques. The major and basic demand of modern techniques is to get homogeneity in the size of particles through which they can be examined easily. The preparation of ceramics with a form of polycrystalline method is classified into the material in the initial state, gaseous phase, and phase of solid or liquid [34]. In the liquid phase, the way to change the solution into a solid state. The best way of liquid phase technique is a sol-gel method. In the solid phase, the method to prepare ceramics powder into two forms, mechanically way, and chemically way. The mechanical method is by ball milling processes, where the chemical way is sol-gel and combustion methods, etc. These are included, but this method is not good for non-oxides and is costly [35]. The mechanical method, compared to the chemical method, is a cheaper and easier way to synthesize lead-free ceramics [36].

2.1.2 Solid State Route

Solid state reaction is a useful method to prepare the lead-free polycrystalline form of ceramics. At room temperature in SSR, route precursors do not respond. To help precursors for the reaction, supply temperature from 1150-1170 degrees centigrade. At the beginning of preparation, the precursors are weighed according to the ratio of materials through which the chemical stability is achieved. If any of them is sensitive to the atmosphere, it can be controlled by the prepared in an evacuated tube. The material heats up into the furnace at 100^oC to remove moisture. To control the homogeneity in the mixture, it can mix mechanically. By milling processes, the particle area decreases easily up to 10μm [37]. For a further decrease in the size of powdered particles, acetone is used as a medium in the milling process for sufficient purity. The formation of phase at a certain temperature is different from TGA. The further step is the reaction between starting material at a certain temperature, this is known as calcination [38].

(a) Precursors

For the formation of lead-free polycrystalline form material, precursors must be highly pure and smooth grain powder. Impurities are directly related to the formation of the desired material, where fine grain material increases reaction because of enhancement of surface area [39]. For the production of materials, their nature exists of much importance. Therefore, the selection of the reactant is very important on behalf of the product nature [40].

(b) Weighing and Ball milling

According to the ratio, precursors are weighted in required figures from coveted compounds. After weighing, mix the material with the help of a ball milling process for some

*Corresponding Author: **Asfand Yar Shafique**

hours. Normally, for the milling medium, acetone and distilled water are used. For drying, the material is placed into the furnace and ground the powder for equality in the size of particles or material [39]. After that, the material gets ready for another process called calcination.

(c) Calcination

The calcination process is also known as firing. In the calcination process, it is required to control the stoichiometry of the material. In the Sintering, the shrinkage of material is observed by the calcination, it can be controlled easily and can be converted into a desirable shape. This shaping is called a green body. Calcination also refers to the formation phase temperature, which comes from the TGA of milled material or (powder) [40]. Precursors of the raw materials dissociate by interdiffusion among various ions. Through the calcination, we can reach the desired phase of ceramics. For the thermal process, that is essential to use the inert body, which does not react easily with the material at very high temperatures. Crucible is the best option as an inert body made up of porcelain or noble metal (Gold, Platinum), etc.

(d) Shaping

For desirable shaping of the calcined material, again, ball milled. The adhesive agent is added to the powder to maintain a dry shape and its strength. There are many shaping methods, such as dry pressing and silk screening, the easy way to prepare simple and small shaping of powder is known as dry pressing. The drying press consists of a movable top and cavity at the lower end. Select the die for shaping and the desired size. Then, open the filled shoe and inject the powder into the die. The material pressed by the punch at the top of the machine, mechanically or hydraulic.

(e) Sintering

The calcined materials are mixed with the adhesive agent solution and then pressed mechanically or as per need for a pellet. The pellets are heated again below the melting temperature of the material for the desired microstructure. For the burning of adhesive agents or binders, the temperature of sintering must be greater than the calcination temperature. The temperature is directly related to the formation of the pellet. Generally, the densification increases with the sintering process [35]. Mechanical cracks were observed clearly by the dry pressing process after sintering. In 1992, *Zheng et al.* observed calcination of boehmite at 400 degrees, showing 73% transformation densification (T.D). At 1000 degree centigrade show, T.D near to 80%. But calcined at 1200 degrees centigrade, the T.D value reduced up to 75%, showing that the densification also depends on nature and phases.

(f) Polishing and Electrode

After the sintering, the sample of pellets is polished for the symmetrically and shiny smooth surfaces. The sample was washed with acetone and then pasted with silver paste. Conduction materials are also used for pasting, like gold, etc. Polished material dried with heat treatment for several minutes at sintered temperature. The sample was pasted with an electrode to study the dielectric properties and polarization.

2.2 Synthesis Lead-Free Lanthanum Doped BNBT

2.2.1 Material

For the preparation of lead-free material with victorious polycrystalline form, their purity has a significant part. The reagents used in the present thesis are bismuth oxide, Titanium oxide, Sodium carbonate, Barium carbonate, and Lanthanum oxide for the vaporization of moisture, placed precursors in the oven for 12 hours at 100^{o}C. The purity and further information of precursors are summarized in following table 1

Table 1. Starting reagents used in the preparation of La-doped BNBT ceramics.

S.No	Chemical Name	Chemical Formula	Purity (%)
1	**Bismuth (III) Oxide**	Bi_2O_3	99
2	**Sodium Carbonate**	Na_2CO_3	98.8
3	**barium Carbonate**	$BaCO_3$	99
4	**Titanium Oxide**	TiO_2	99
5	**Lanthanum (III) Oxide**	La_2O_3	99

2.2.2 Preparation of Lead-Free Ceramics Powder

To prepare the solid solution of $[(Na_{0.5}\ Bi_{0.5})_{0.94}\ Ba_{0.06}]0.98\ La0.02TiO_3$ (BNLBT) powder with the method of conventional solid-state reaction. The powder consist of (Bi_2O_3, Na_2CO_3, $BaCO_3$, TiO_2, La_2O_3) initial raw material. Stoichiometrically weighed the materials mixed materials by ball milling for 24 hours under the ethanol, where a ZrO2 ball was used as a media. The prepared solution was further treated at a temperature of 100^{o}C for 12 hours to dry with the help of an electric oven. Calcination of powder is performed in a crucible at 850^{o}C for 2 hours. After calcination, once again, the ball was milled for 24 hours because the calcined powder became agglomerated, and to break this agglomeration, we attempted the ball milling process a second time. The powder of BNLBT was mixed with a solution of polyvinyl alcohol (PVA) and converted into a green disk 10 mm in diameter by mechanical pressed by the pressure of 100 MPa; then the green disk was sintered at the temperature of 1150^{o}C for 2 hours. The flow chart for the preparation sample is shown in Figure 2.1.

*Corresponding Author: **Asfand Yar Shafique**

Figure 2.1 Flow chart of solid state route method for La-doped BNBT ceramics.

After preparation of the lead-free ceramic La-doped BNBT, The crystal structure and lattice parameters of the sample were using an X-ray Diffractometer (XRD, X'Pert-PRO MRD, Philips, KBSI). By lapping, the surface of a sintered sample is removed. The lapped sample was gently polished and thermally etched at 1050°C for 30min. Finally, field emission scanning electron microscopy (FE-SEM Hitachi.S-4200 & Japan) was used for the surface morphological study of the doped sample. On both sides of the green disk, silver paste was applied. After pasting, the disk was fired at 700 ◦C for 30 min. The hysteresis loop of the dopped sample was calculated in silicon oil with the aid of a Sawyer–Tower circuit to apply a field (Electric Field) with a sinusoidal waveform. The electric-field-induced strain was measured by a linear variable differential transducer (LVDT, Mitutoyo MCH-331 & M401).

2.3 X-ray Diffraction (XRD)

The X-ray diffraction in crystals was first explained by Max Von Laue in 1912. The technique was developed by W.H. Bragg and his son W. L. Bragg. In the beginning, the Laue analysis was assumed, X-ray diffraction referent three-dimensionally spread atoms in rows. That assumption was not wrong but difficult to understand. Bragg and his son also explained, based on assumption but were quietly different from the Laue, that the atoms of the crystal are spread three-dimensionally in different planes and where the angle of incident and angle of reflection are equal to each other. This assumption was correct based on their geometry but not satisfied with physical perception because x-rays are not reflected from the layer of the atom [39].

XRD is used for the determination of the arrangement of the atoms within a crystal. In XRD, the monochromatic beam of x-ray bombards directly on a sample, where the rays spread in many directions. The X-rays are produced with the help of a cathode ray tube. When the x-rays fall on the material, incident and diffracted rays produce constructive interference when obeying Bragg's Law ($n\lambda=2d\sin\theta$) shown in Figure 2.2 X-ray produced diffraction peaks [40].
Where,

n = Order or number of diffraction
λ = Wavelength of Incident beam of X-ray
d = Interplanar distance or lattice plane distance
θ = Diffraction angle

The surface morphology is examined by the XRD spectra. Every sample contains a specific pattern of XRD. By the XRD, we can identify whether the samples are crystalline or polycrystalline. In a single crystal, all the unit cells show regularity, where the polycrystalline has a smooth plane surface. The peak values of the spectra help to study the cell parameters, interplanar space, and shape of the unit cell. The interplanar space has a direct relation with the lattice parameter.

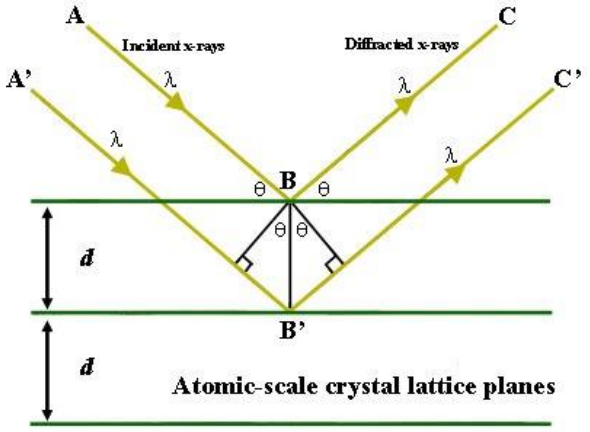

Figure 2.2 Diagram of X-ray contact with crystal lattice planes**.**

The peak value also gives information about the crystallite size and imperfection in the lattice**.** The sharp peaks are referred to calculate the lattice parameter, assigning values of (h,k,l) by the relation of [41].

$$h^2/a^2 + k^2/b^2 + l^2/c^2 = 1/d^2_{hkl} \quad \text{2.1 (a)}$$

or

$$(h^2/a^2 + k^2/b^2 + l^2/c^2)\, d^2_{hkl} = 1 \quad \text{2.1 (b)}$$

2.4 Scanning Electron Microscope (SEM)

One of the skilled instruments accessible for the study of the microstructural characteristics of solid materials is the scanning electron microscope (SEM). SEM is widely used in many fields of science because of its high resolution during the examination of bulk material, commercially instrumental values in order of 2nm-5nm (20Å to 50Å). While for the present high-tech research instrument is preceded to a resolution better than 10Å or 1nm. The SEM consists of lenses, an electron gun (source), an electron collector

*Corresponding Author: **Asfand Yar Shafique**

(detector), a screen, and a cathode ray tube (CRT), and the electronics circuit is shown in Figure 2.3. SEM is the technique that is used to get data about topography, morphology, defects, and the composition of the solid material, as well as crystallographic information. SEM contains a focused number of electrons with high energies to make images of the solid material by raster scan. The collected information is from the desired area of the solid material, and a 2-D image is produced. The beam of electron bombard on the sample contains kinetic energy. The incident beam of electrons loses kinetic energy while penetrating the material, and the continuous X-ray is produced with all possible wavelengths related to the incident beam electron energies. The accelerated beam shows the number of signals when it interacts with the atom of the solid sample. For example, backscattered electrons (BSE), BSE was also known as primary electron. At the same time, the secondary electron (SE) is generated in the form of photons or ions due to incident energy. The signals are not generated at the origin; it is produced within the volume of the sample called interaction volume (IV).

The incident beam of electrons covered some distance inside the solid material during penetration, the electron scattered back outside of the material called backscattered electrons (BSE), either elastic or inelastic. BSE is important to show the composition in multiphase of the material. The incident beam of electrons produces the SE during the ionization process in the solid material, which is important for morphology and topography. The key point for studying the prepared sample in SEM is that the material must be electrically conductive. The non-conductive material should be coated with conducting material, for example, chromium, graphite, gold, etc. The non-conducting ceramics charged automatically during the scanning process by the beam of the electron, where the error was observed in the secondary electron image frame. SEM techniques are known as non-destructive techniques because the volume loss factor of the prepared material during analysis is scarce.

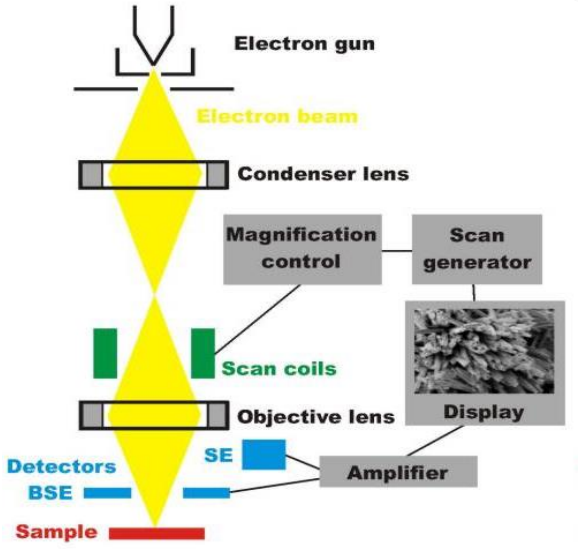

Figure 2.3 Schematic diagram of Scanning electron microscope schematic diagram.

2.5 Field Emission Scanning Electron Microscope (FE-SEM)

Field emitter is preferred comparatively thermionic emission because when in thermionic emitter, filament (tungsten) is heated enough to overcome the work function of the filament material, the electrons escape from the material. Thermionic emission has drawbacks of little brightness, evaporation of cathode material, and thermal drift during operation. To avoid these kinds of problems, we preferred Field emission source. FES does not heat the material and is also called a cold cathode field emitter. Therefore, FES combines with SEM, which encourages advancing the secondary electron technology.

Electrons emitted from the FES (Field emission Source) called primary electron. Which accelerated in strong electrical field gradient. Within the vacuum, these electrons are focused and produce narrow scan beam by deflection of electronic lenses. After that secondary electron are emitted at each point from the object. While the structure of the object is depend upon the velocity and angle of the secondary electron. Detector detects the secondary electron and make electronic signal. These signal transformed a digital image that can be seen on computer screen. The FE-SEM consists of high energetic beam of electron through which clear magnified image. FESEM used to measure the thickness of film, height of the nanometer sized object, surface, and defect analysis.

2.6 Dielectric Measurements

When dielectric material or insulator is placed between the two electrodes, by the External electric field dipole induce into the insulator or dielectric material. Dielectric materials polarized in opposite direction to external field and produced an electric field inside the dielectric materials. The capacitance of the capacitor for storing charges is enhanced due to the dielectric material placed between the two plates compared to the vacuum or medium (air). The value of the dielectric constant shows the capability of the high storage medium. Near to low applied voltage to ignore the 180-degree movement of the domain, ferroelectric substances are studied for dielectric properties [42].

2.6.1 Dielectric Polarization

The separation of charges induced by the applied external field within the dielectrics is called polarization. The polarization in the insulator/dielectrics is mathematically expressed as

$$P = \propto E \qquad 2.2$$

'P' stands for polarization of dielectric material, 'E' for external field, and '$\propto$' the polarizability of the material [43]. Total polarizability within the material '$\propto_\tau$' is cause by the effect of these four types, ionic '$\propto_i$', electronic '$\propto_e$', dipolar '$\propto_d$', and Interfacial polarizabilities '$\propto_f$' as given in the following equation.

$$\propto_\tau = \propto_i + \propto_e + \propto_d + \propto_f \qquad 2.3$$

(a) Ionic Polarization

Positive and negative ions are disturbed from their equilibrium state in the ionic under the applied field called

ionic polarization. The cations and anions get closure to the oppositely charged plates and increase the net dipole moment. This type of polarization is directly affected by changing the temperature. The ionic polarization leads to transition, a transition due to ionic polarization in the crystal material known as a displacive phase transition. The displacement of ions, which is comparatively heavier than the electron, can be easily achieved from 10^{12} to 10^{13} Hz (Infrared frequency).

(b) Electronic Polarization

The Positive charges or nucleus and negative charges or electrons of an atom slightly displaced due to the applied field are known as electronic polarization, as shown in Figure 2.4. Generally, mathematically, the electronics polarizability expressed as the dipole moment of charges is directly proportional to the number of charges per unit volume and the force of the applied field. The electronic polarizability is independent of temperature and achieved from 10^{15} to 10^{16} Hz (visible-UV Frequency) [44].

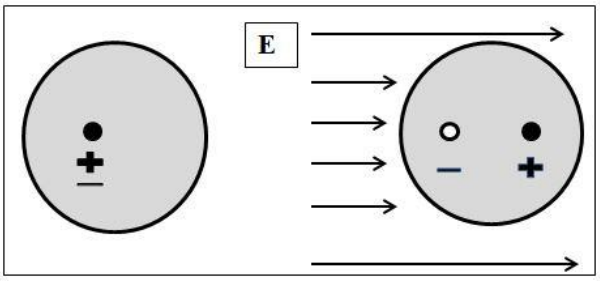

Figure 2.4 Electronic polarization

(a) Dipolar Polarization

The effect caused by the external electric field is that when Polar molecules are placed into the strong field, the orientation of the permanent dipole moment orient in the direction of the external field this process is called dipolar or orientational polarization. The strength of the externally applied field is directly proportional to the alignment of the permanent dipole. When the strength of the applied field increases, the alignment of the dipoles develops in the direction of the applied external electric field. The resistance proposed by the atom or molecule to the displacement of charges or orientation of dipole in the applied field helps to measure polarizability. When a dielectric material is placed in the applied external field, each dipole experiences the torque singly, which can align in the field direction. The polarization of dielectric material is inversely proportional to the temperature, the polarization of dielectric material decreases with increasing temperature. With increasing temperature, the vibrational energy of molecules is enhanced. As a result, the dipole alignment is disturbed.

(b) Interfacial Polarization

External applied electric field with small frequency, cause to move charge from one place to another place through the material. The process in which the movement of charges is impeded within the interfaces of material is known as interfacial polarization. In interface polarization, the permittivity can be enhanced by a trap of the charges within interfaces, where the movement of charges stops when charges are not freely discharged. These accumulations of charges enhance the capacitance. If the particle layers are slim and their dimensions are much smaller, at low applied frequency, maximum charges accumulate near the conduction region, causing an increase in the permittivity. At large applied frequencies, the charges have no time to accumulate; the polarization is negligible because of the small charge displacement compared to the conduction region [45]. Interfacial polarization occurs in low frequency, and responses range (10-3 to 103Hz) at very high temperatures. Because of the very large temperature, the dislocation in the material occurs, which refers to interfacial polarization.

3. Dielectric Constant

The theory of dielectric was put forward by Michael Faraday in 1837. Faraday performed experimental work to examine the effect of dielectric between the electrodes under the DC source. The ability of the material to store charges under the external electric field is known as a dielectric. Faraday observed that the storing charge capacity of the capacitor of parallel plates with the dielectric material shows maximum storage value comparatively the capacitor without medium between plates [46]. In an idealized capacitor, the area of parallel plates denoted by 'A,' separating distance parallel plate' and with variable potential 'V' induce the charge density 'D' mathematically expressed as

$$D = \varepsilon_o V/d \qquad 3.1$$

'ε_o' is the permittivity of free space, the mathematical value of 'ε_o' is 8.85 X 10^{-12}F/m.

The dielectric constant can be written as below:

$$\varepsilon_r = \varepsilon' - I\varepsilon'' \qquad 3.2$$

The dielectric constant has two components: real and imaginary. In 0^o phase difference with an applied electric field, ε' is the real component. While at 90 phase difference under the external field, ε'' is the imaginary component of the dielectric constant phase difference of 90^o under the applied external field. The phase difference in the imaginary part is caused by leakage in the dielectric material. The dielectric constant with a high peak is observed for the ferroelectric material compared to organic and inorganic solids [42].

3.1 Dielectric Loss

When the A.C. voltage is applied to the dielectric material, the energy absorbed by the material is converted into thermal energy. This loss of energy is known as dielectric loss and is also called the dissipation factor. There is no consumption of energy into the perfect insulator or dielectric material. In a real insulator or dielectric material under the applied field, the energy storage of charges and loss of current must be produced, this loss of energy appears because of the movement of charges through the material at a large distance. The dissipation of energy is related to the rotation or vibration of dipoles [42]. Without ideal dielectric material, the loss factor may be contained in all types of dielectric materials.

*Corresponding Author: **Asfand Yar Shafique**

3.2 Temperature Dependence of Dielectric Constant and Loss Factor

As we studied in previous literature, ferroelectric material contains huge dielectric properties compared to non-ferroelectric material. The studies of dielectric properties for the ferroelectric material proceed with the research of the desired material. The values of the material studied through the low field are beneficial for measuring the capacitive as well as desired piezoelectric material. The changing of temperature helps to examine easily transition phases and depolarization. The temperature independence permittivity measurement helps to differentiate between relaxor behavior and normal ferroelectric.

3.3 Diffuse Phase Transition

The transition temperature is not clearly defined in the homogenous material. The analysis of DPT is calculated from the dielectric constant vs temperature graph, which is established in the ferroelectric material. At very high temperatures near phase transition temperature, the diffuseness of phase is considered because of fluctuation. There are two types of fluctuation: compositional and structural fluctuation. Thermodynamics explains clearly that the ferroelectric solid material contains compositional fluctuation, which occurs because of small changes of energy between the huge and low-temperature phases near the transition temperature. Where the chances of fluctuation increase because of a change of small disturbance between the ferroelectric and paraelectric phases. *Fritsberg et al.* observed that stability is inversely proportional to the diffuse transition, less the stability of material a hoped large diffusion transition [47]. In the complicated perovskite structure of ferroelectric materials, the disarrangement of cation shows diffuse phase transition, where the maximum temperature-dependent values can be measured for relative permittivity 'εr' and dissipation factor in the transition region [48]. Mathematically, it can be explained as

$$1/\varepsilon - 1/\varepsilon_m = (T-T_m)^{\square}/C \qquad 3.3$$

'T_m' is the maximum temperature at which the maximum dielectric constant peak reaches, 'γ' is the diffuse factor, and 'C' is the constant of curie called curie constant. 'γ' ranges lies between 1 to 2 if the γ = 1 which shows the normal ferroelectric phase transition and obeys Curie–Weiss law. If the γ = 2, it shows complete diffusion because of the compositional fluctuation [49,51].

4. Result and Discussion

4.1 Structural Analysis by XRD

X-ray diffraction (XRD) pattern of La-doped BNBT sample in the 2θ degree range 20^o – 90^o is shown in figure 4.1(a). The plotted pattern of XRD showed a single perovskite rhombohedral structure without another secondary phase. Moreover, La was replaced with A-site, and it was suggested that the doping level was quite low, which completely dissolved. This implies that the addition of lanthanum diffuses into the crystal lattice and forms a pure BNBT solid solution, where the sample clearly shows typically ABO_3 perovskite diffraction peaks. The magnified XRD figure (b) at 2□□□of □□^{o} displayed showed a broad peak with a rhombohedral symmetry.

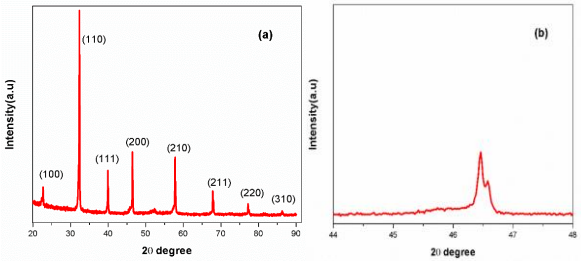

Figure 4.1(a) XRD plots of La 0.02mol% doped in BNBT piezoelectric ceramics.
(b) 2θ degree range from 44^o – 48^o.

4.2 Surface Morphological Study

Morphological study of material of the La 0.02mol% doped in BNBT done with help of field-emission scanning electron microscope. This technique makes it easy to study the surface of the material shown in Figure 4.2. La-doped in BNBT ceramic showed irregularly shaped grains with clear grain boundaries. This fine microstructure transpires homogeneity and, without any impurities, is fully dense. The average grain size of ceramic La-doped in BNBT was measured by the method of linear intercept. The average grain size for La 0.02 mol% is 1.08 to 2.02 µm. Usually, piezoelectric materials require a huge mechanical strength. For the improvement of mechanical strength and densification of the piezoelectric material, uniform grain and regular size of grain play a very important role.

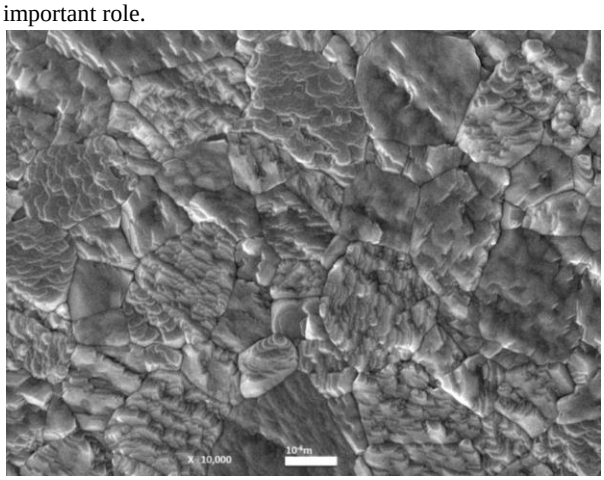

Figure 4.2 FE-SEM images for surface analysis.

4.3 Temperature Dependence of Relative Permittivity (εr) and Loss Factor (tanδ)

The temperature-dependent relative permittivity at 1kHz, 10kHz, 100kHz, and 1MHz is shown in Figure 4.3. Lanthanum doped 0.02mol% in BNBT shows two different dielectric anomalies, usually positioned at T_d and T_m. The T_d stands for depolarization temperature, which is similar to the transition from FE to AFE state. T_m is the highest temperature, where the maximum relative permittivity (ε_r) reaches, which is similar to the transition from AFE to paraelectric state or cubic. Under the 1kHz frequency, the maximum ε_r value 3714 is obtained at T_m= 252°C, where the T_d is observed at 110°C. Under 10kHz frequency, the maximum ε_r value decreases

from 3714 to 3646 at T_m= 252°C, but there was a very small change occurring in T_d. At 100kHz frequency, ε_r slightly decreases from 3646 to 3641 at T_m= 248-250°C. The huge change observer at T_m= 248°C, under the 1MHz frequency maximum relative permittivity, increases from 3641 to 3980, where the T_d vanished and dielectric peaks broader. The broader peaks refer to phase transition as diffuse phase transition at maximum temperature T_m, which is observed in various ABO_3 perovskite structures and BNT systems [51].

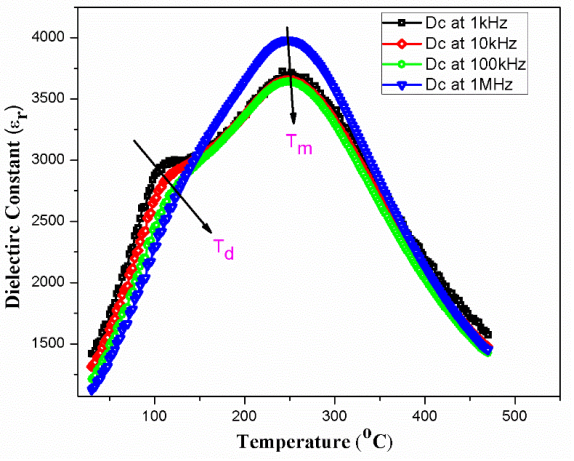

Figure 4.3 Temperature dependence of ε_r at various frequencies.

The temperature-dependent loss Factor (tanδ) was obtained at 1kHz, 10kHz, 100kHz and 1MHz frequencies. Temperature dependence tanδ values were observed at 1kHz frequency, where the loss was 0.043 or 4.3% at 30°C and gradually enhanced with increased temperature. The loss peak at 1kHz decreases from 94-138°C, where loss decreases from 0.048 to 0.004 or 4.8% to 0.4%, then loss increases with increasing temperature, as shown in figure 4.4.

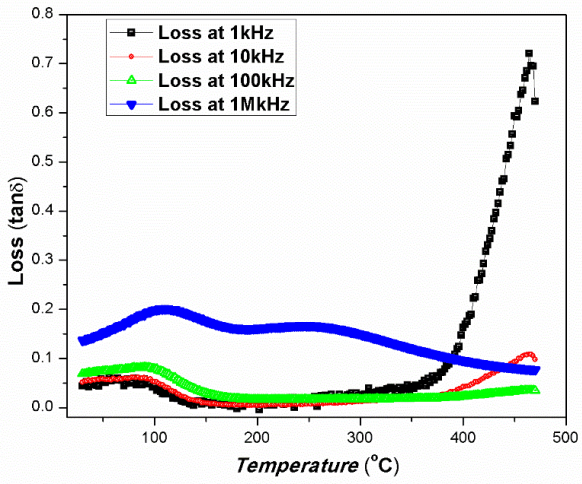

Figure 4.4 Loss tanδ at various frequencies of La 0.02mol% doped in BNBT.

For 10kHz, 0.05 or 5% loss was obtained at 30°C, and a slightly large value was observed with increased temperature, the loss located peak at 10kHz decreases from 94-202°C, where loss reached from 0.057 to 0.0046 or 5.7% to 0.46%. After the temperature of 202°C, loss gradually increases. For 100kHz, 0.0689 or 6.8% loss was observed. At 98 to 218°C, the loss value decreases from 0.079 to 0.016 or 7.9% to 1.6 %. After 202°C under the 100kHz frequency, loss values with small differences remain approximately the same with an increase in temperature. For 1MHz, 0.137 or 13.7% loss was observed at 30°C, where the different peak positions were located between 114°C and 248°C with a maximum loss factor from 0.20 to 0.16 or 20% to 16%. These different positions of peaks were observed in many other ceramics. The widened loss tanδ in various frequencies at high temperatures probably occurs because of space charge polarization [52]—the unified graph of temperature dependences of ε_r and tanδ shown in Figure 4.5.

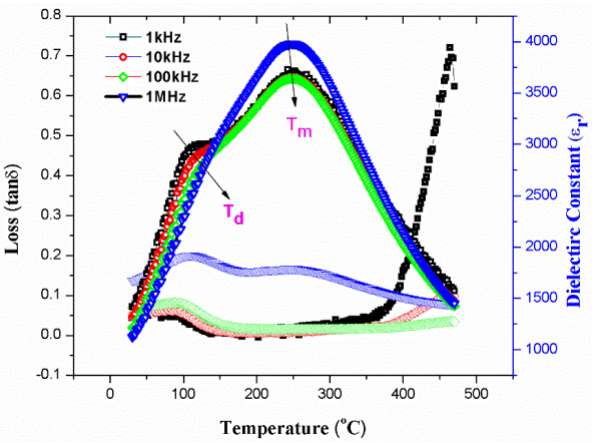

Figure 4.5 Temperature dependence of ε_r and tanδ of La 0.02mol% at various frequencies.

4.4 Diffusive Factor (γ)

For the 0.02mol% La-doped BNBT system, the graph plot between log $(1/\varepsilon_r\text{-}1/\varepsilon_m)$ vs log$(T\text{-}T_m)$ under the variation of different frequencies from 1kHz to 1MHz is shown in Figure 4.6.

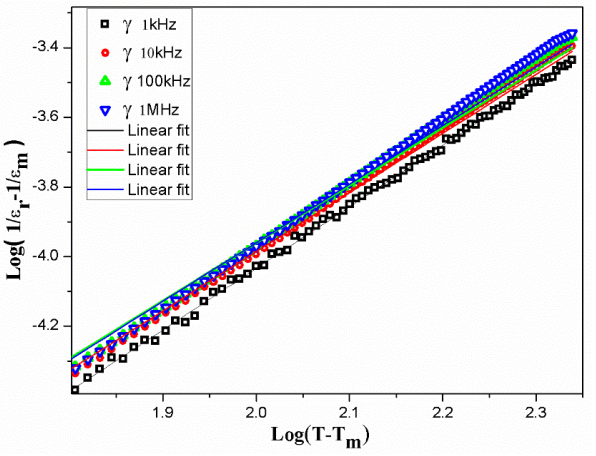

Figure 4.6 La 0.02mol% doped BNBT plot between log (1/εr-1/εm) vs log(T-Tm).

'ε_r' is the relative permittivity, 'ε_m' is the maxima of relative permittivity, 'T' stands for temperature, and 'T_m' is the maximum temperature at which the 'ε_r' value achieved maximum value. 'γ' is the diffusivity factor, which shows the dependence of the material with composition and structure.

*Corresponding Author: **Asfand Yar Shafique**

The quantity of 'γ' calculated from the slope of linear fitting of the acquired data from log $(1/\varepsilon_r - 1/\varepsilon_m)$ vs log$(T-T_m)$. The 'γ' values for the 0.02mol% La-doped BNBT are shown in Table 4.1. The sample with 0.02mol% of La with different frequencies, where 'γ' values lie between 1 and 2, shows the nature of the sample with diffusive phase transition and relaxor of ferroelectric system. The 'γ' values decrease with increasing the applied field from 1kHz to 100kHz but slightly increase at 1MHz.

Table 4.1 Diffusive factor 'γ' values under various frequencies.

Applied Frequency	Diffusive Factor 'γ'	Standard Error
1 kHz	1.76	0.006
10 kHz	1.69	0.009
100 kHz	1.65	0.0141
1 MHz	1.68	0.012

4.5 Piezoelectric Analysis (Bipolar Strain)

Figure 4.7 shows the piezoelectric constant d33 of the 0.02mol% La dopped BNBT lead-free ceramics sintered at 1150oC. The highest strain, Smax= 0.27% under 70 kV/cm and d33* (Smax/Emax)= 387 pm/V, are obtained. La dopped BNBT shows a butterfly-shaped strain curve, typically examined in ferroelectric ceramics.

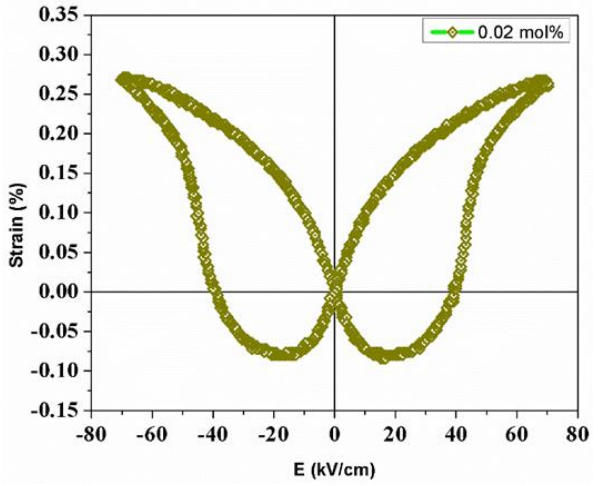

Figure 4.7 S-E loop for La 0.02mol% doped BNBT

4.6 P-E Loop Study

P-E loops are measured for the analysis of the ferroelectric nature of 0.02mol% La-doped BNBT lead-free ceramic, as shown in Figure 4.8.

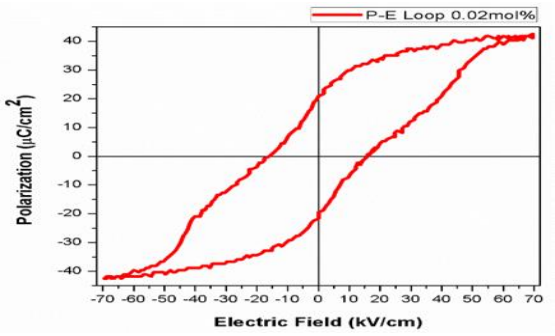

Figure 4.8 P-E loop for La 0.02mol% doped BNBT.

The maximum polarization (P_{max}), remnant polarization (P_r), and coercive field (E_c) of the La-doped BNBT sample sintered at 1150°C, the value obtained under the field of 70 kV/cm, P_{max}= 42.58 μC/cm^2, P_r= 20.91 μC/cm^2 and E_c= 16 kV/cm observed. According to the thermodynamic theory of ferroelectric, huge remnant polarization generally promotes an increase in piezoelectric properties.

Experimental analysis shows that the P-E loop is very slim, which shows that 0.02mol% La-doped BNBT lead-free ceramic is an excellent ferroelectric material with good remnant polarization, low coercive field, and high saturation polarization. When an external field is applied, the material aligns easily in the direction of the field and returns to its initial state after the field is removed.

Conclusion

The prepared sample lead-free piezoelectric ceramics La 0.02 mol% doped BNBT shows excellent piezoelectric response. The XRD diffraction shows the pure single perovskite rhombohedral structure. Generally, rhombohedral structures exhibit ferroelectric characteristics by applying an external strong field to the specimen. The prepared sample exhibits typically ABO_3 perovskite diffraction peaks. The addition of lanthanum in BNBT densifies the material, which is seen with proper clear grain boundaries. The average grain size of the examined sample is La 0.02mol%, which is 1.08 to 2.02μm. Where the strength of the material increases with a dopant. A huge dielectric constant examines 3980 for 0.02mol% under the maximum applied field (1MHz), where the depolarization temperature peak becomes vanishes. With the addition of lanthanum 0.02mol%, the low loss factor (tanδ) observed tanδ < 10%, large maximum strain S_{max} is 0.27% observed, a huge normalized strain d_{33}*= 387 pm/V under 70 kV/cm at room temperature. Slim P-E loop is obtained for BNBT-La 0.02mol%, from P-E loop huge remnant polarization P_r= 20.91 μC/cm^2, maximum polarization P_{max}= 42.58 μC/cm^2 and coercive field E_c= 16 kV/cm observed.

References

1. Devonshire, A. F. (1949). XCVI. Theory of barium titanate: Part I. The London, Edinburgh, and Dublin Philosophical Magazine and Journal of Science, 40(309), 1040-1063.
2. Nidhi Verma, Satyendra Singh, B.C. Yadav, Experimental investigations on barium titanate nanocomposite thin films as an optoelectronic

*Corresponding Author: **Asfand Yar Shafique**

humidity sensor, J of Experimental Nanosci. 1(2012) 1-9.
3. Tadashi Takenaka, Piezoelectric properties of some lead-free ferroelectric ceramics, Ferroelectrics, 230 (1999) 87-98.
4. Jones, G. O., & Thomas, P. A. (2002). Investigation of the structure and phase transitions In the novel A-site substituted distorted perovskite compound $Na_{0.5}Bi_{0.5}TiO_3$. Acta Crystallographica Section B: Structural Science, 58(2), 168-178.
5. Yan, H., Xiao, D., Yu, P., Zhu, J., Lin, D., & Li, G. (2005). The dependence of the piezoelectric properties on the differences of the A-site and B-site ions for $(Bi_{1-x}\ Na_x)\ TiO_3$-based ceramics. Materials & Design, 26(5), 474-478.
6. Li, Y., Chen, W., Zhou, J., Xu, Q., Sun, H., & Xu, R. (2004). Dielectric and piezoelectric properties of lead-free $(Na_{0.5}Bi_{0.5})TiO_3$–$NaNbO_3$ ceramics. Materials Science and Engineering: B, 112(1), 5-9.
7. Li, Y., Chen, W., Zhou, J., Xu, Q., Sun, H., & Liao, M. (2005). Dielectric and ferroelectric properties of lead-free $Na_{0.5}Bi_{0.5}TiO_3$–$K_{0.5}Bi_{0.5}TiO_3$ ferroelectric ceramics. Ceramics International, 31(1), 139-142.
8. Yoshii, K., Hiruma, Y., Suzuki, M., Nagata, H., & Takenaka, T. (2007). The Piezoelectric Properties of La_2O_3 Doped $(Bi_{1/2}Na_{1/2})TiO_3$–$(Bi_{1/2}K_{1/2})TiO_3$ Ceramics. Ferroelectrics, 358(1), 134-138.
9. Xu, Q., Xie, J., He, Z., Zhang, L., Cao, M., Huang, X., ... & Liu, H. (2017). Energy-storage properties of $Bi_{0.5}Na_{0.5}TiO_3$-$BaTiO_3$-$KNbO_3$ ceramics fabricated by wet-chemical method. Journal of the European Ceramic Society, 37(1), 99-106.
10. Wada, S., Yamato, K., Pulpan, P., Kumada, N., Lee, B. Y., Iijima, T., ... & Kuroiwa, Y. (2010). Piezoelectric properties of high Curie temperature barium titanate–bismuth perovskite-type oxide system ceramics. Journal of Applied Physics, 108(9), 094114.
11. Takenaka, T., Maruyama, K. I., & Sakata, K. (1991). $(Bi_{1/2}Na_{1/2})TiO_3$-$BaTiO_3$ system for lead-free piezoelectric ceramics. Japanese Journal of Applied Physics, 30(9S), 2236.
12. Ranjan, R., & Dviwedi, A. (2005). Structure and dielectric properties of $(Na_{0.50}Bi_{0.50})_{1-x}\ Ba_xTiO_3$: $0 \leq x \leq 0.10$. Solid state communications, 135(6), 394-399.
13. Balakt, A. M., Shaw, C. P., & Zhang, Q. (2017). Giant pyroelectric properties in La and Ta co-doped lead-free $0.94Na_{0.5}Bi_{0.5}TiO_3$-$0.06BaTiO_3$ ceramics. Journal of Alloys and Compounds, 709, 82-91.
14. Balakt, A. M., Shaw, C. P., & Zhang, Q. (2017). The decrease of depolarization temperature and the improvement of pyroelectric properties by doping Ta in lead-free $0.94Na_{0.5}Bi_{0.5}TiO_3$-$0.06BaTiO_3$ ceramics. Ceramics International, 43(4), 3726-3733.
15. Xia, X., Jiang, X., Chen, C., Jiang, X., Chen, Y., Tu, N., & Jiang, Y. (2017). Enhanced piezoelectric performance and orange-red emission of Sm^{3+} doped $(Na_{1/2}Bi_{1/2})$ TiO3-based lead-free ceramics. Ceramics International, 43(1), 376-384.
16. Liao, Y., & Xiao, D. (2009). Synthesis and electrical properties of Li-modified $Bi_{0.5}Na_{0.5}TiO_3$-$BaTiO_3$ lead-free piezoelectric ceramics. Journal of materials science & technology, 25(6), 777-780.
17. Lee, J. K., Yi, J. Y., & Hong, K. S. (2004). Dependence of incommensurate phase formation on vacancy type in La-doped $(Na_{1/2}Ba_{1/2})TiO_3$. Journal of Applied Physics, 96(2), 1174-1177.
18. Kim, J., Kim, S., Choi, B., Jeong, J., No, Y., Chung, S., & Son, S. (2009). Effect of La Doping on the Dielectric and the Ferroelectric Properties of Lead-Free $Na_{1/2}Bi_{1/2}TiO_3$ (NBT) Ferroelectric Ceramics. Journal of Korean Physical Society, 54, 911.
19. Mercadelli, E., Galassi, C., Costa, A. L., Albonetti, S., & Sanson, A. (2008). Sol-gel combustion synthesis of BNBT powders. Journal of Sol-Gel Science and Technology, 46(1), 39-45.
20. Qu, Y., Shan, D., & Song, J. (2005). Effect of A-site substitution on crystal component and dielectric properties in $Bi_{0.5}Na_{0.5}TiO_3$ ceramics. Materials Science and Engineering: B, 121(1), 148-151.
21. Rao, K. S., Rajulu, K. C. V., Tilak, B., & Swathi, A. (2010). Effect of Ba^{2+} in BNT ceramics on dielectric and conductivity properties. Natural Science, 2(04), 357.
22. Chen, F., Liu, Q. X., Tang, X. G., Jiang, Y. P., Yue, J. L., & Li, J. K. (2016). Diffuse phase transition and high-temperature dielectric relaxation study on $(Bi_{0.5}Na_{0.5})1\text{-}x\ Ba_xTiO_3$ ceramics. Physica B: Condensed Matter, 496, 20-25.
23. Fu, Peng, Zhijun Xu, Ruiqing Chu, Xueyan Wu, Wei Li, and Xiaodong Li. "Structure and electrical properties of $(1-x)(Na_{0.5}Bi_{0.5})0.94\ Ba0.06TiO_3$–$xBiAlO_3$ lead-free piezoelectric ceramics." Materials & Design 46 (2013): 322-327.
24. Zhao, Y., Xu, J., Zhou, C., Yuan, C., Li, Q., Chen, G., & Yang, L. (2016). High energy storage properties and dielectric behavior of $(Bi_{0.5}Na_{0.5})0.94\ Ba0.06Ti_{1-x}(Al_{0.5}Nb_{0.5})_xO_3$ lead-free ferroelectric ceramics. Ceramics International, 42(2), 2221-2226.
25. Cheng, R., Xu, Z., Chu, R., Hao, J., Du, J., & Li, G. (2016). Electric field-induced ultrahigh strain and large piezoelectric effect in $Bi_{1/2}Na_{1/2}TiO_3$-based lead-free piezoceramics. Journal of the European Ceramic Society, 36(3), 489-496.
26. Wang, C., Xu, Z., Cheng, R., Chu, R., Hao, J. Li, W, & Li, G. (2016). Electric field-induced giant strain and piezoelectricity enhancement effect in $(Bi_{1/2}Na_{1/2})0.935 + xBa_{0.065}\ Ti\ 1-x(Pr_{1/2}Nb_{1/2})_xO_3$ lead-free ceramics. Ceramics International, 42(3), 4354-4360.

27. Hao, J., Xu, Z., Chu, R., Li, W., Fu, P., & Du, J. (2016). Field-induced large strain in lead-free $(Bi_{0.5}Na_{0.5})_{1-x}$ $Ba_xTi0.98(Fe_{0.5}Ta_{0.5})0.02O_3$ piezoelectric ceramics. Journal of Alloys and Compounds, 677, 96-104.
28. Li, L., Hao, J., Chu, R., Xu, Z., Li, W., Du, J., & Fu, P. (2016). Dielectric, ferroelectric and field-induced strain response of lead-free (Fe, Sb)-modified $(Bi_{0.5}Na_{0.5})0.935Ba0.065TiO_3$ ceramics. Ceramics International, 42(8), 9419-9425.
29. Zheng, Q., Xu, C., Lin, D., Gao, D., & Kwok, K. W. (2008). Piezoelectric and ferroelectric properties of $(Bi_{0.94-x}La_xNa_{0.94})0.5$ $Ba0.06TiO_3$ lead-free ceramics. Journal of Physics D: Applied Physics, 41(12), 125411.
30. Yamamoto, T. (1992). Optimum preparation methods for piezoelectric ceramics and their evaluation. American Ceramic Society Bulletin, 71(6), 978-985.
31. Arlt, G. (1990). The influence of microstructure on the properties of ferroelectric ceramics. Ferroelectrics, 104(1), 217-227.
32. Carter, C. B., & Norton, M. G. (2007). Ceramic materials: science and engineering. Springer Science & Business Media.
33. Bonner, W. A., & Zydzik, G. J. (1970). Growth of single crystal lead molybdate for acousto-optic applications. Journal of Crystal Growth, 7(1), 65-68.
34. Ring, T. A. (1996). Fundamentals of ceramic powder processing and synthesis. Academic Press, 2 81-82.
35. M. N. Rahaman, Ceramic Processing and Sintering (Second Edition, 2003). 64-67, 369-373.
36. Jonscher, A. K. (1999). Dielectric relaxation in solids. Journal of Physics D: Applied Physics, 32(14), R57.
37. Electroceramics, A. J. (1990). Moulson and JM Herbert. Chapman & Hall, ISBN 0-412-29490-7, 621, M92e.
38. G.C.C. da Costa, A.Z. Simões, A. Ries, C.R. Foschini, M.A. Zaghete, and J.A. Varela: Mater. Lett., 2004, vol. 58, pp. 1709–14.
39. Hammond, C., & Hammond, C. (2001). Basics of crystallography and diffraction (Vol. 214). Oxford.
40. Smart, L. E., & Moore, E. A. (2005). Solid state chemistry: an introduction. CRC press.
41. Suzuki, E. (2002). High-resolution scanning electron microscopy of immunogold-labelled cells by the use of thin plasma coating of osmium. Journal of Microscopy, 208(3), 153-157.
42. Jeffe, B., Cook, W. R. and Jaffe, H. 1971. Piezoelectric ceramics, New York: Academic.
43. Bunget, I., & Popescu, M. (1984). Physics of solid dielectrics (Vol.19). Elsevier Science Ltd.
44. Nussberger, M. (2005). Soil moisture determination with TDR: single-rod probes and prfile reconstruction algorithms (Doctoral dissertation).
45. Note, A. A. (2006). Agilent Basics of Measuring the Dielectric Properties of Materials. Agilent Literature Number.
46. Tayal D. C., (1988). Electricity and Magnetism. New Dehli, India. Himalaya Publishers,
47. Jonker, G. H. (1983). On the dielectric curie-weiss law and diffuse phase transition in ferroelectrics. Materials Research Bulletin, 18(3), 301-308.
48. Tang, X. G., Wang, J., Wang, X. X., & Chan, H. L. W. (2004). Effects of grain size on the dielectric properties and tunabilities of sol–gel derived $Ba(Zr_{0.2}Ti_{0.8})O_3$ ceramics. Solid State Communications, 131(3), 163-168.
49. Tilak, B. (2012). Ferroelectric relaxor behavior and spectroscopic properties of Ba^{2+} and Zr^{4+} modified sodium bismuth titanate. American Journal of Materials Science, 2(4), 110-118.
50. Shukla, A., & Choudhary, R. N. P. (2010). Ferroelectric phase-transition and conductivity analysis of La^{3+}/Mn^{4+} modified $PbTiO_3$ nanoceramics. Physica B: Condensed Matter, 405(11), 2508-2515.
51. Li, Y., Chen, W., Xu, Q., Zhou, J., Gu, X., & Fang, S. (2005). Electromechanical and dielectric properties of $Na_{0.5}Bi_{0.5}TiO_3$–$K_{0.5}Bi_{0.5}TiO_3$–$BaTiO_3$ lead-free ceramics. Materials Chemistry and Physics, 94(2), 328-332.
52. Palei, P. K., & Kumar, P. (2012). Role of Sintering Temperature on the Phase Stability and Electrical Properties of $0.94(K_{0.5}Na_{0.5}NbO_3)$–0.06 $(LiSbO_3)$ Ceramics. Japanese Journal of Applied Physics, 51(1R), 011503.

*Corresponding Author: **Asfand Yar Shafique**